Modeling Charge Preparation and Combustion in Diesel Fuel, Ethanol, and Dual-Fuel PCCI Engines

Sage L. Kokjohn*, Derek A. Splitter, Reed M. Hanson, and Rolf D. Reitz
Department of Mechanical Engineering
University of Wisconsin-Madison
Madison, WI 53706 USA

Vittorio Manente and Bengt Johansson
Division of Combustion Engines
Department of Energy Sciences
Lund University, Sweden

Abstract

Premixed charge compression ignition (PCCI) has been shown to be a promising strategy to simultaneously reduce NOx and soot emissions while realizing improved fuel economy. PCCI combustion uses high levels of pre-combustion mixing to lower both NOx and soot emissions by ensuring low equivalence ratio and low flame temperatures. The high level of pre-combustion mixing results in a primarily kinetics controlled combustion process. Because reaction rates are very sensitive to temperature and equivalence ratio, modeling of PCCI combustion requires precise treatment of the injection, evaporation, and mixing processes.

In this work multi-dimensional CFD modeling predictions are compared for three different methods of achieving PCCI combustion. The first method is early injection, highly dilute (i.e., low oxygen concentration), diesel fuel PCCI operation. In this method, the oxygen concentration is reduced to extend the ignition delay to allow adequate time for mixing prior to auto-ignition. The second method is early injection PCCI operation using neat ethanol. In this method, the fuel reactivity is sufficiently low that PCCI combustion can be achieved without using external dilution. The final method, dual-fuel PCCI combustion, blends two fuels with varying reactivity in the combustion chamber to tailor the auto-ignition properties of the mixture for the specific operating condition.

It was found that the modeling approach used in this work is capable of capturing the bulk combustion characteristics (e.g., cylinder pressure) as well as the details of the injection event (e.g., liquid penetration) and ignition processes. The simulations were shown to provide accurate predictions of the differences in combustion characteristics of diesel fuel, ethanol, and blends of gasoline and ethanol with diesel fuel. It was found that the ethanol PCCI and dual-fuel PCCI cases have significantly reduced rates of energy release compared to neat diesel fuel PCCI operation. The reduced energy release rates of the ethanol PCCI and dual-fuel PCCI cases may allow these modes of PCCI combustion to achieve higher engine loads than that of neat diesel PCCI.

* Corresponding author: kokjohn@wisc.edu

Introduction

Increasingly stringent emissions regulations and a focus on the reduction of green house gases have driven the development of advanced combustion technologies that can simultaneously yield high efficiency and low emissions. Many of the current strategies can be lumped into the category of low temperature combustion (LTC) [1-3]. In low temperature combustion the ignition delay is extended such that significant pre-combustion mixing occurs; thus, soot emissions are reduced by avoiding overly rich regions. Additionally, by allowing sufficient mixing time, the peak equivalence ratios can be reduced and, therefore, low flame temperatures can be achieved and the formation of thermal NOx can be avoided. Low temperature combustion strategies range from fully premixed operation (e.g., Sjoberg et al. [4]) to partially premixed operation (e.g., Manente et al. [5]). Premixed charge compression ignition (PCCI) is a form of low temperature combustion, which generally features early cycle injections and high-levels of pre-combustion mixing. In this work the terms low temperature combustion and premixed charge compression ignition (PCCI) will be used interchangeably.

In recent years, much attention has focused on which fuel is best for LTC or PCCI combustion. Kalghatgi et al. [6, 7] operated a compression ignition engine on gasoline and found that the decreased fuel reactivity (i.e., increased resistance to auto-ignition) extended the ignition delay, which resulted in significantly lower NOx and soot than operation using neat diesel fuel. Although, the increased ignition delay of gasoline allows NOx and soot reductions at mid- to high-load operating points, it can be difficult to achieve auto-ignition at light engine loads. Bessonette et al. [8] explored the effects of fuel reactivity on compression ignition operation over a range of engine loads. Their work suggested that as the engine operating conditions (e.g., speed and load) are changed, the optimum fuel reactivity may change. Similarly, Kokjohn et al. [9], Hanson et al. [10], and Splitter et al. [11] used kinetics modeling, detailed CFD, and engine experiments to access the fuel reactivity requirements with changing engine loads. They found that by blending gasoline and diesel fuel in-cylinder, high-efficiency, low-emissions operation could be achieved over a range of conditions.

In recent years computer modeling using detailed CFD coupled with reduced kinetics schemes has become a key step in the engine design process. The use of computer modeling allows engine designers to explore advanced combustion strategies first on a computer before expensive hardware is manufactured. Additionally, modeling results can provide access to information that is difficult or impossible to measure directly. As combustion strategies become more and more complex, it is important to compare modeling predictions to measured results to ensure accurate predictions are being made as modeling is used to explore unconventional combustion strategies.

Scope and Objectives

In this work, detailed CFD modeling results are compared to engine experiments operating in the LTC combustion regime using three different fuels or blends of fuels (diesel fuel, ethanol, and gasoline-ethanol-diesel fuel blends).

First, model predictions are compared to an engine operating in the LTC combustion mode using neat diesel fuel. In this case, the engine modeled was an optically accessible heavy-duty type diesel engine and comparisons between the model predicted and measured charge preparation and early cycle reactions are presented. Next, comparisons are made to a PCCI engine fueled by neat ethanol. After that, modeling predictions are compared to an engine operating in dual-fuel PCCI combustion mode. In this low temperature combustion strategy, a relatively un-reactive fuel is premixed using port-fuel-injection and a more reactive fuel is delivered using direct-injection. In this work fuel property effects are evaluated by comparing two cases: dual-fuel PCCI operation using port-fuel-injection of neat gasoline and direct-injection of diesel fuel and dual-fuel PCCI operation using port-fuel-injection of a blend of 85% ethanol and gasoline (E85) and direct-injection of diesel fuel. In each of these cases the model predictions are evaluated and discussed. In the final section of this study, the modeling results are used to compare the three LTC operating strategies.

Computational Model

Computations are performed using the KIVA-3v release 2 code [12] with improvements to many physical and chemistry models developed at the ERC [13-15]. The KIVA-3v code is coupled with the CHEMKIN II solver for detailed chemistry calculations. A 49 species and 179 reaction mechanism describing the oxidation of iso-octane, n-heptane, and ethanol [16] was used to simulate gasoline, diesel fuel, and ethanol chemistry, respectively. Many studies (e.g., Ra et al. [17]) have shown the combustion characteristics of gasoline and diesel are represented well by iso-octane (i.e., PRF 100) and n-heptane (i.e., PRF 0), respectively. This approach has also been shown to yield acceptable agreement for blends of gasoline and diesel fuel (e.g., Kokjohn et al. [9]). The physical properties (for the spray and mixing processes) of diesel fuel are represented by tetradecane. This modeling approach has been shown to yield acceptable results in numerous studies (e.g., Kong et al. [18]) and

is further validated in this work. Soot is predicted using a phenomenological soot model [18] based on the approach of Hiroyasu [19]. The soot model used in the present study uses acetylene as the soot inception species, which allows the soot model to be coupled to the chemistry solver through the addition of 13 reactions involving acetylene. NOx emissions are predicted using a reduced NO mechanism [20] consisting of 4 additional species and 12 reactions. The reduced NO mechanism is based on the Gas Research Institute (GRI) NO mechanism [21].

The spray model employed in this study uses the Lagrangian-Drop and Eulerian-Fluid (LDEF) approach. Because a detailed chemistry model is used, it is desirable to use a relatively coarse computational mesh; however, severe grid size dependency has been observed in LDEF spray models. This problem is most severe in the near nozzle region where the droplets are very close together and occupy only a small portion of the Eulerian mesh. Abraham [22] showed that accurate modeling of the near nozzle region required grid resolution on the order of the orifice diameter. However, it is not feasible from a computational time standpoint to solve engine problems on such a fine mesh. In order to reduce the grid size dependency of the LDEF spray model and allow accurate spray simulation on a relatively coarse grid, the Gasjet model of Abani et al. [14] is used to model the relative velocity between the droplets and gas phase in the near nozzle region.

Droplet breakup is modeled using the hybrid Kelvin Helmholtz (KH) – Rayleigh Taylor (RT) model described by Beale et al. [23]. The droplet collision model is based on O'Rourke's model; however, a radius of influence method is used to determine the possible collision partners to further reduce mesh dependency [14]. In addition, the collision model was expanded by Munnannur [24] to include a more comprehensive range of collision outcomes. The current implementation of the droplet collision model considers bounce, coalescence, and fragmenting and non-fragmenting separations. Droplet interactions with the wall are considered through a wall film submodel [25, 26], which includes the effects associated with splash, film spreading, and motion due to inertia.

Engine Specifications and Operating Conditions

Experimental data using a single engine operating over this span of low temperature combustion strategies was not available. Therefore, data was taken from the literature from three different engines. The specifications for each engine are shown in Table 1. The first set of comparisons is made to a heavy-duty engine based on a Cummins N14 operating in an early injection LTC combustion mode. The experiments were performed by Singh et al. [27]. This engine has been extensively discussed in the literature (e.g., Musculus [28]); thus, for brevity, no discussion is made here. The neat ethanol PCCI experiments were performed by Manente et al. [29] using a Scania D12. A detailed description of this engine and the experimental setup can be found in [29]. The gasoline-diesel dual-fuel PCCI experiments were performed by Hanson et al. [10] and the E85-diesel dual-fuel experiments were performed by Splitter et al. [30]. Both sets of dual-fuel PCCI experiments were conducted using a Caterpillar heavy-duty single-cylinder research engine. Again, since this engine has been extensively discussed in the literature, the engine specifications are presented in Table 1 with no additional discussion. The computational sector grid for each engine represents a single injector hole. The grids for the three engines are shown in Figure 1.

Table 1. Engine specifications.

Case	Diesel LTC [27]	Ethanol PCCI [29]	Dual-Fuel PCCI [10, 30]
Engine	Cummins N14	Scania D12	CAT SCOTE
Displacement (cm3)	2340	1966	2440
Stroke (mm)	152.4	154	165.1
Bore (mm)	139.7	127.5	137.2
Con. Rod (mm)	304.8	255	261
CR (-)	11.2	14.3:1	16.1
Swirl Ratio (-)	0.5	2.9	0.7
Number of nozzles	8	8	6
Nozzle hole size (μm)	196	180	250

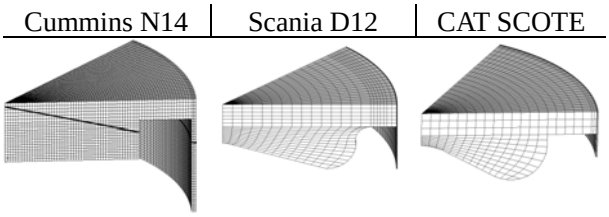

Figure 1. Computational grids for the three engines modeled in this study.

The operating conditions for each case are presented in Table 2. Notice that the cases using ethanol (i.e., the ethanol PCCI and E85-diesel dual-fuel PCCI combustion cases) are able to operate without using EGR (i.e., the inlet O_2 concentration is 21%) due to the low reactivity of ethanol as well as the reduced

temperatures due to the high latent heat of vaporization of ethanol. In the case of diesel LTC and gasoline-diesel dual-fuel PCCI, EGR or intake dilution is required to ensure combustion does not occur too early in the cycle. Additionally, notice that the diesel LTC and ethanol PCCI cases feature a single early cycle injection, while the dual-fuel PCCI cases use a split-early cycle injection to ensure optimal fuel distribution.

Table 2. Operating conditions.

Case	Diesel LTC [27]	Ethanol PCCI [29]	Dual-Fuel PCCI [10, 30]	
Fuel	Diesel	Ethanol	E85-Diesel	Gasoline-Diesel
Speed (RPM)	1200	1300	1300	1300
IMEP (bar)	3.9	5	9.6	9.6
Intake Temp (°C)	90[1]	157	44	32
Intake Pressure (kPa)	214	140	201	174
Rail Pressure (bar)	1600	1800	800	800
SOI 1 (°ATDC)	-22	-60	-58	-58
SOI 2 (°ATDC)	-	-	-39	-37
Fraction of fuel in pulse 1	1.0	1.0	0.6	0.6
Total fuel quantity (mg)	56	71	123	94
Gasoline mass %	0	0	24	89
Diesel mass %	100	0	22	11
Ethanol mass %	0	100	54	0
IVC Timing (°ATDC)	-165	-151	-85	-143
Inlet O2 (Vol. %)	12.7	21	21	15.9
EGR (Vol. %)	NA[2]	0	0	43

[1] To allow optical access an extended piston assembly is used, which results in a relatively low geometric compression ratio (see Table 1). To simulate TDC conditions of a heavy-duty type diesel engine with a compression ratio of 16:1, the intake temperature and pressure were increased above typical values for this operating condition.

[2] The optical engine used in [27] was skip-fired to reduce thermal loading. Because of the skip-fired operation, dilution using recirculated exhaust gas (EGR) was not possible. Therefore, the intake oxygen concentration was diluted with N_2 to reduce flame temperatures and delay combustion phasing.

Simulation Results and Discussion

Early Injection PCCI Combustion

Figure 2 shows a comparison between the measured [27] and predicted cylinder pressure and apparent heat release rate (AHRR) for the early injection, LTC diesel combustion case. In this case, the injection timing is sufficiently advanced (compared to conventional diesel operation) and the inlet O_2 has been reduced such that the end-of-injection (EOI) occurs prior to the start-of-combustion. The simulations do an adequate job capturing the ignition delay and combustion duration. Notice that, due to the significant pre-combustion mixing, the combustion process is primarily premixed. That is, very little mixing controlled combustion is observed. Additionally, it can be seen that, even with very dilute operation (i.e., low intake O_2 concentration) combustion occurs significantly before top-dead-center. The early combustion phasing is due to the high-reactivity of diesel fuel.

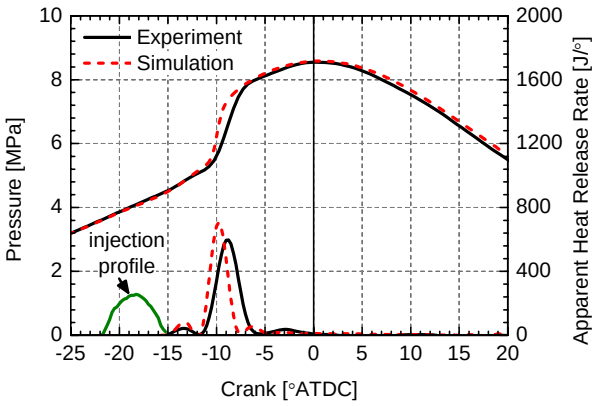

Figure 2. Comparison of measured and predicted cylinder pressure and AHRR for the early-injection LTC diesel combustion case. The measured cylinder pressure and AHRR of Singh et al. [27] are shown in solid black lines, the calculated cylinder pressure and AHRR are shown with red dashes.

Singh et al. [27] simultaneously acquired single-shot images of liquid fuel and line-of-sight natural emission images for early-injection LTC operation. These images are used to validate model predicted spray penetration and early stage combustion. In the experiments first stage ignition was identified by naturally occurring luminous emission. To differentiate first-stage ignition, second-stage ignition, and soot luminosity, Singh et al. [27] relied on the relative change in emission intensity (i.e., the required camera gain). They showed that for first-stage ignition the required camera gain was on the order of 10^5, for

second-stage ignition the required camera gain was on the order of 10^3, and for soot luminosity the camera gain was near 1.

Lachaux et al. [31] have shown that formaldehyde (H_2CO) tracks well with the "soup" of hydrocarbons formed during the early stage reactions. Thus, formaldehyde was used to mark the location of first stage ignition in the simulations. As the charge transitions to second stage ignition, a buildup of OH radicals is observed. Therefore, in the simulations, second stage ignition was marked by the location of OH radicals. As the combustion process continues, soot precursors are formed in fuel rich regions. In the current simulations acetylene (C_2H_2) is used as a soot precursor. Thus, acetylene was used as a marker for regions likely to form soot.

Figure 3 shows the comparison of the first stage ignition process for the early injection LTC diesel combustion case. The top row of images are from the experiments of Singh et al. [27] and the bottom row of images are the modeling results. Note that only a single nozzle hole was modeled in this study; however, to allow comparisons with the experimental images, the modeling results were duplicated to show five of the eight fuel jets. In both the experimental and computational images the field of view focuses on a single fuel jet looking upward through a quartz piston window. The liquid fuel is shown in blue for both the experiments and simulations. The experimentally observed naturally occurring luminous emission is shown in green and the relative camera gain is shown in the upper right-hand corner of each image. In the simulations, formaldehyde is shown in light green, OH is shown in bright green, and acetylene (a soot precursor) is shown in red. The white dot on the left side of each image shows the location of the fuel injector nozzle and the white curve on the right side of each image shows the location of the piston bowl rim. The crank angle, in degrees after the start-of-injection (ASOI), is shown in the lower left-hand corner of the images.

At 7 and 7.5 °ASOI the experiments show weak chemiluminescence (camera gain on the order of 1e5) on the outer edge of the spray plume. Notice that, in the experiments, it is difficult to see the luminescence in the three o'clock jet in the 7 °ASOI image; however, Singh [27] points out that the jets on both sides (i.e., one o'clock and five o'clock) appear to show luminescence on the outer edges. In good agreement with the observed luminescence, the simulations show first stage ignition occurs first on the outer portions of the jet. Further notice that the simulations reproduce the liquid penetration very well.

At 10° ASOI it can be seen that first stage ignition occurs throughout the jet cross section. This is shown by the weak luminescence (camera gain on the order of 1e5) in the experiments and location of formaldehyde in the simulations. At 12 °ASOI, the camera gain in the experiments must be reduced by two orders of magnitude to avoid saturation. This increase in luminosity suggests a transition to second stage ignition. At this point luminosity is observed mainly at the location where the jet interacts with the piston bowl. The increase in luminosity likely signals a transition to second stage ignition and the presence of luminous soot. In good agreement with the observed results, the simulations show the presence of soot precursors in the jet-bowl interaction region. Additionally, the simulations show a transition to second stage ignition (signaled by the buildup of OH radicals) occurs at the near the location of jet-bowl interaction.

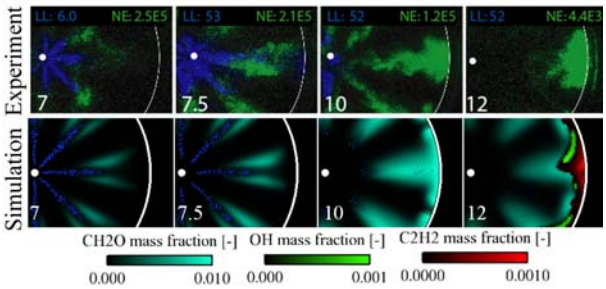

Figure 3. Comparison of single–shot broadband natural emission images [27] with computed contours of formaldehyde, OH, and acetylene for the LTC-long ignition delay condition.

Early Injection PPCI Combustion Using Neat Ethanol

Figure 4 shows a comparison of the measured [29] and predicted cylinder pressure and AHRR for the case operating in early injection PCCI combustion mode using neat ethanol. It can be seen that the simulations do a reasonable job capturing the ignition delay; however, the peak pressure is slightly over-predicted. This is also observed in the AHRR, where it can be seen that an over-prediction in the early stages of energy release is observed. At this point, it is unclear whether the slight over-prediction in the rate of heat release is due the kinetics model, charge preparation, or boundary conditions (e.g., wall temperature). However, it should be pointed out that the peak pressure was sensitive to the specified wall temperature. Although some minor differences exist, the simulations do a reasonable job capturing the combustion characteristics of ethanol PCCI combustion at this condition. Notice that both the simulations and experiments show relatively long combustion duration, which is uncharacteristic of premixed compression ignition.

With confidence in the model predictions, the simulations were used to understand the spray, mixing, and ignition processes of ethanol PCCI combustion.

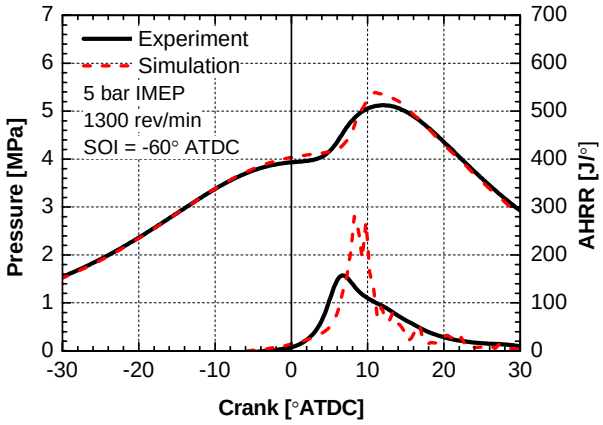

Figure 4. Comparisons of measured [29] and predicted cylinder pressure and AHRR for an engine operating on neat ethanol in PPCI combustion mode.

Specifically, it is of interest to understand the observed relatively long combustion duration for ethanol PCCI operation. This is particularly interesting because it may allow higher load PCCI operation to be achieved, while maintaining moderate rates of pressure rise. Figure 5 shows cut-planes colored by equivalence ratio and temperature. It can be seen that the injection targets the piston bowl rim and the fuel is nearly equally distributed between the bowl and squish regions. Due to the very advanced injection timing, significant pre-combustion mixing occurs and by the time of auto-ignition, the peak equivalence ratio is ~0.5. The very low equivalence ratio results in relatively low flame temperatures and very low NOx emissions.

Ignition occurs in the center of the piston bowl in a region with an equivalence ratio of ~0.3. This finding is unintuitive, since fuel reactivity generally increases with equivalence ratio. However, in the case of direct injected ethanol, the significant charge cooling that

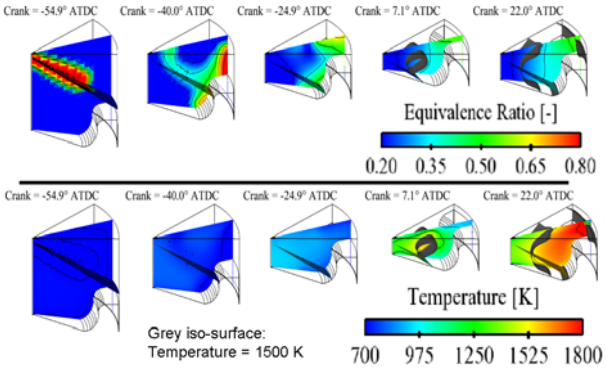

Figure 5. Cut-planes colored by equivalence ratio (top) and temperature (bottom) for an engine operating in PPCI combustion mode using neat ethanol. The iso-surface corresponds to a temperature of 1500 K.

occurs during the injection event causes the richest regions of the chamber to be the coldest and thus ignition occurs in a leaner region near the center of the combustion chamber. The reaction zone then consumes the richer-cooler regions in the outer-portion of the combustion chamber. Thus, it appears that the observed extended combustion duration is due to thermal stratification generated during the direct-injection event.

Dual-Fuel PCCI combustion using blends of gasoline and diesel fuel and blends of E85 and diesel fuel

Figure 6 shows a comparison of the measured and predicted cylinder pressure and apparent heat release rates for operation at 9.6 bar IMEP and 1300 rev/min using both E85-diesel fuel blends and gasoline-diesel fuel blends. Notice that the operating conditions have been selected such that the combustion phasing is the same between the two cases. It can be seen that the simulations do an excellent job capturing the combustion characteristics for both the gasoline-diesel fuel blend as well as the E85-diesel fuel blend. More specifically, notice that the change in combustion characteristics between the gasoline-diesel blend and the E85-diesel blend is captured very well by the simulations. That is, dual-fuel PCCI combustion using a blend of E85 and diesel fuel shows a nearly "triangular shaped" heat release profile and a very broad combustion duration.

The simulations are used to further understand the differences in combustion characteristics between dual-fuel operation using the two different fuel blends. Figure 7 shows the evolutions of several key species for both fueling strategies. It can be seen that, in general, the combustion processes between gasoline-diesel fuel and E85-diesel fuel blends are very similar. Specifically, n-heptane (diesel surrogate in computation) is consumed early in the cycle resulting in a significant buildup in formaldehyde, which was also experimentally validated in [11]. As the combustion processes transition to second stage ignition, a simultaneous consumption in formaldehyde, isooctane, and, in the case of E85-diesel fuel blends, ethanol is observed. However, several differences can be found. It appears that the consumption of n-heptane is delayed for the ethanol-diesel fuel blends compared to the gasoline-diesel fuel blends. The delayed consumption of n-heptane for the E85-diesel fuel case results in a delay in the buildup of formaldehyde. Additionally, the transition to second stage ignition (signaled by the consumption of formaldehyde and buildup in OH radicals) occurs slightly earlier for the ethanol-diesel fuel blends. Although, the transition to second stage ignition occurs slightly earlier, the buildup in OH

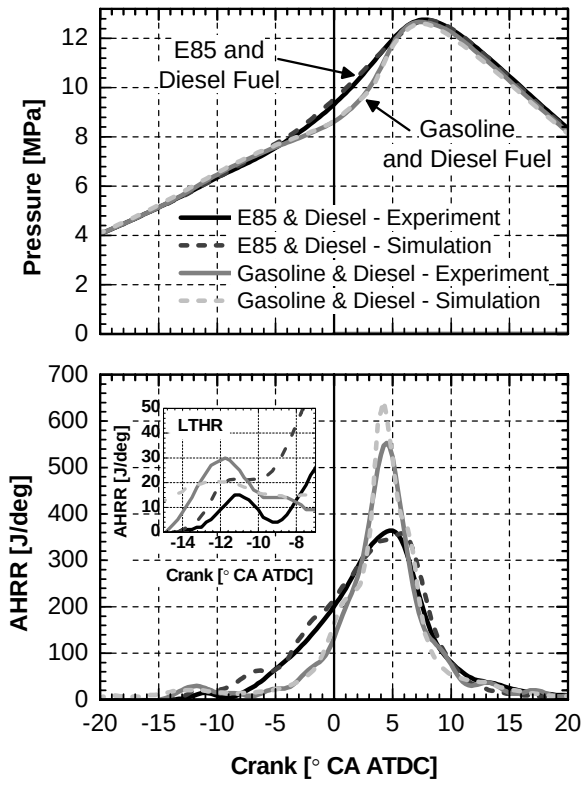

Figure 6. Comparison of measured [10, 30] and predicted cylinder pressure and apparent heat release rate (AHRR) for dual-fuel PCCI combustion operating on E85-diesel fuel and gasoline-diesel fuel blends. The solid lines are from the experiments and the dashed lines are the modeling predictions. Note the differences in low and high temperature heat release rates with E85 as compared to gasoline port fueling, even with twice as much diesel fuel used with E85.

radicals is much more gradual for the E85-diesel fuel blends compared to the gasoline-diesel fuel cases.

Hashimoto [32] performed detailed kinetics calculations and found that ethanol had a significant inhibitor effect on the cool flame chemistry of heptane mixtures. He attributed this inhibitor effect to consumption of OH radicals by the ethanol molecule. In another work [33], Hashimoto observed that the ethanol inhibitor effect significantly delayed the second stage heat release of heptane mixtures. The results of Figure 6 and Figure 7 are consistent with the findings of Hashimoto [32, 33]. That is, although significantly higher quantities of diesel fuel (n-heptane in the simulations) were used in the E85-diesel fuel cases compared to the gasoline-diesel fuel cases, the cool flame energy release was significantly reduced. Additionally, the buildup in formaldehyde was delayed for E85-diesel fuel blends. Finally, it appears that the presence of ethanol as the diesel fuel transitions to second stage ignition is at least partially responsible for the observed extended combustion duration.

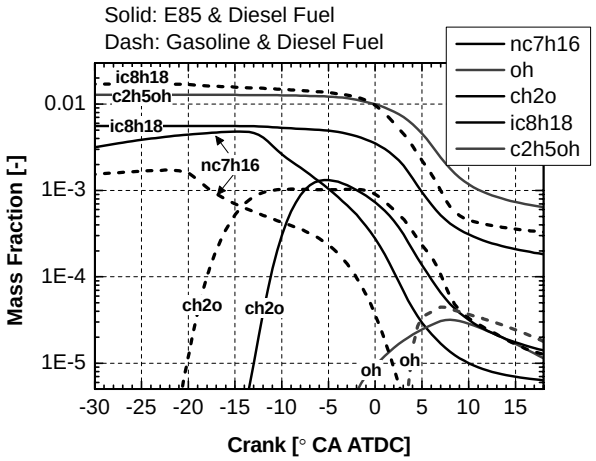

Figure 7. Evolutions of n-heptane (nC7H16), iso-octane (iC8H18), ethanol (C2H5OH), formaldehyde (CH2O), and the hydroxyl radical (OH) for E85-diesel fuel blends (solid curves) and gasoline-diesel fuel blends (dashed curves). Note that in the simulations n-heptane is used to represent diesel fuel and iso-octane is used to represent gasoline.

As previously mentioned, it is thought that the ethanol inhibitor effect is partially responsible for the extended combustion duration observed for E85-diesel fuel blends. However, the dual-fuel charge preparation strategy described in [34] results in an in-homogeneous fuel species distribution, due to the port-fuel-injection of gasoline or E85 and direct-injection of diesel fuel. Specifically, stratification in fuel reactivity exits. To understand the influences of the stratified fuel reactivity on the extended heat release for E85-diesel fuel blends, the fuel reactivity distributions of gasoline-diesel and E85-diesel operation were compared. Assigning a research octane number (RON) of 107 to ethanol [35], an overall fuel RON can be defined as:

$$\mathrm{RON} = \frac{100 x_{\mathrm{isooctane}} + 107 x_{\mathrm{ethanol}}}{x_{\mathrm{isooctane}} + x_{\mathrm{nheptane}} + x_{\mathrm{ethanol}}} \qquad (1)$$

where x is the mole fraction of each fuel species. Note that, as previously discussed, Hashimoto [32, 33] has shown that ethanol has a significant inhibitor effect on the oxidation of n-heptane; therefore, assigning a reactivity to blends of ethanol and n-heptane may not be as straightforward as presented in Eq. 1. Nevertheless, it is informative to understand the fuel distribution prior to auto-ignition. Figure 8 shows cut-

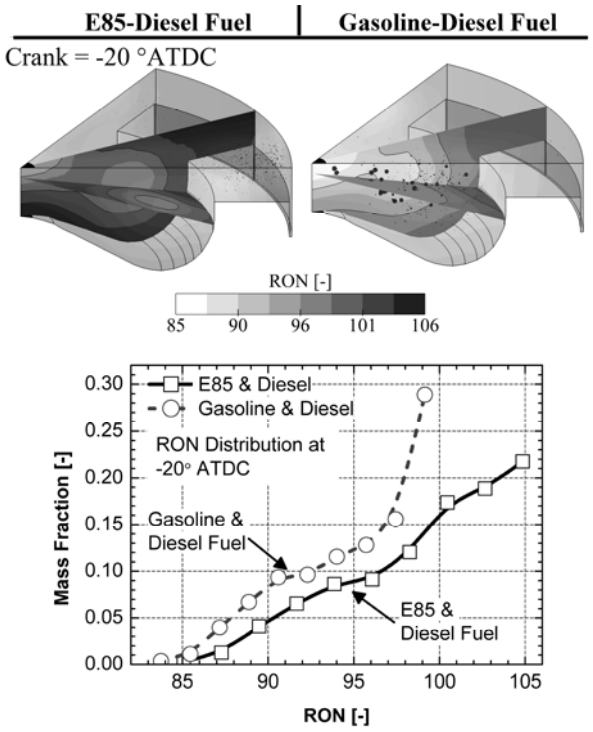

Figure 8. Contours colored by RON, see Eq. 1, on cut-planes coincident with the spray axis and the mass distribution of RON at 20° BTDC. The mass fraction shows the fraction of the mass in the combustion chamber at the specified RON.

planes shaded by RON and the mass distribution of RON at 20° BTDC, near the time when n-heptane consumption begins due to low-temperature reactions. The mass distribution of RON was calculated by binning the combustion chamber by RON at 20° BTDC (near the time when low-temperature reactions were observed). The mass fraction indicates the fraction of the total combustion chamber mass at the specified RON. It can be seen that the gasoline-diesel fuel blends have slightly more mass as lower RON than the E85-diesel fuel blends. However, it can also be seen that the range of RON encountered in the combustion chamber for the gasoline-diesel fuel blends is lower than that of the E85-diesel fuel blends. That is, the E85-diesel fuel blends have a larger degree of fuel reactivity stratification than the gasoline-diesel fuel blends. Based on the above observations, it appears that the extended combustion duration for the E85-diesel fuel blends is the result of a combination of broader fuel reactivity distributions, the ethanol cooling effect, and the ethanol inhibitor effect described by Hashimoto [32, 33].

Comparisons Between Diesel LTC, Ethanol PCCI, and Dual-fuel PCCI Combustion

The previous sections have shown that the modeling approach used in this work is capable of capturing both the global combustion characteristics (e.g., cylinder pressure) as well as details of the spray and reaction progress. In this section, the simulations are used to compare the three premixed compression ignition (PCI) combustion processes evaluated in this study. Figure 9 shows the calculated AHRR for three PCI cases (diesel LTC, ethanol PCCI, and dual-fuel PCCI using E85 and diesel fuel). The AHRR profiles are presented as a percentage of the total fuel energy per unit time so that energy release rates can be compared for the different engines and operating points. The combustion characteristics are seen to be distinctly different for the three cases.

First, although the diesel LTC case has the latest injection timing and highest level of dilution (i.e., lowest inlet O_2 concentration), the high reactivity of the diesel fuel results in significantly advanced combustion phasing compared to the other two cases. Additionally, it can be seen that rate of heat release is extremely rapid for the diesel LTC case. The rapid rate of energy release is partially attributed to the fact that the combustion occurs prior to top-dead-center. The energy release rate is further increased by a nearly simultaneous auto-ignition event (i.e., nearly all of the fuel reacts at nearly the same time). This is shown by both the experiment and simulation results in Figure 3, where it can be seen that both the low-temperature reactions and high-temperature reactions occur nearly simultaneously throughout the jet-cross section.

The ethanol PCCI case shows the latest combustion phasing and shows a significantly reduced rate of energy release compared to the diesel-LTC operation. From the simulation results presented in Figure 5, it appears that the reduced rate of energy release is partially the result of the late combustion phasing and partially the result of a staged auto-ignition event generated by thermal stratification due to the direct injection. As was previously discussed, the simulation results show that the richest regions of the chamber were significantly cooler than the leaner regions of the combustion chamber. It was shown that the combustion event progressed from the leaner-hotter regions to the richer-cooler regions.

Comparing the above dual-fuel PCCI case to the diesel LTC and ethanol PCCI cases, it can be seen that the combustion initiates only slightly later than the diesel LTC case. However, due to the gradient in fuel reactivity, the rate of combustion is relatively low and the combustion duration is very broad.

To further understand the differences in the

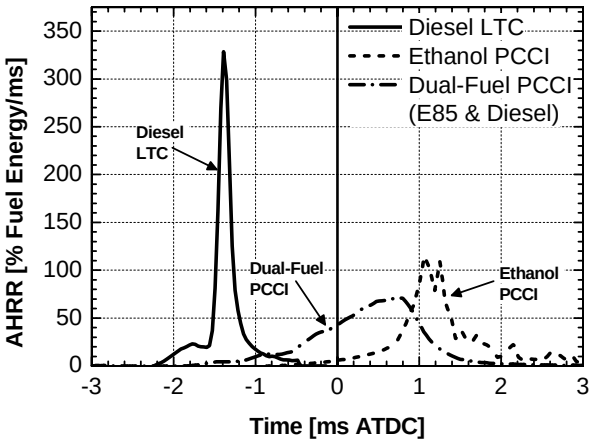

Figure 9. Comparison of the energy release characteristics of diesel LTC, ethanol PCCI, and dual-fuel PCCI. Note that the AHRR's are presented as function of time to account for the differences in engine speed.

combustion processes, Figure 10 shows comparisons of the evolutions of several key species, fuel, formaldehyde (CH_2O), and the hydroxyl (OH) radical. Comparing the species evolutions reveals key differences in the combustion processes. The diesel LTC case shows that formaldehyde is formed during low-temperature reactions, but is quickly consumed as the combustion process transitions to second stage ignition. It can be seen that the temporal differences in diesel consumption and formaldehyde consumption is 0.2 ms (~2° CA at 1200 rev/min.). Notice also, that the buildup in OH is nearly instantaneous. That is, the entire charge transitions to second stage ignition at nearly the same time. Recall that this finding is consistent with the observed rapid energy release in Figure 3.

The ethanol PCCI case shows that formaldehyde forms early in the cycle due to early stage fuel decomposition. However, it can be seen that the level of formaldehyde is significantly lower than either the diesel LTC case or the dual-fuel PCCI case. This finding is expected since ethanol is a single stage fuel. That is, ethanol does not exhibit the two-stage auto-ignition behavior observed for diesel fuel. Further, it can be seen that only a small fraction of the ethanol has been consumed early in the cycle. Comparing the OH profile for the ethanol PCCI case to that of the diesel LTC case, it can be seen that, consistent with the observed reduced heat release rate, the rate of OH buildup is significantly lower.

Finally, comparing the species evolutions for the dual-fuel PCCI case to the previous two cases shows that a significant quantity of formaldehyde is formed early in the cycle due to low temperature reactions of the diesel fuel. However, unlike the diesel LTC case, the delay between the diesel fuel and formaldehyde consumption is approximately 1 ms (~8° CA at 1300 rev/min.). Notice also, that ethanol and iso-octane (gasoline) are consumed nearly simultaneously with formaldehyde. That is, the less reactive fuels are not consumed until the diesel fuel transitions to second stage ignition. Finally, it can be seen that the rate of OH radical buildup is significantly lower for the dual-fuel PCCI case than the other two cases. Again, this finding is consistent with the reduced rate of energy release associated with dual-fuel PCCI combustion.

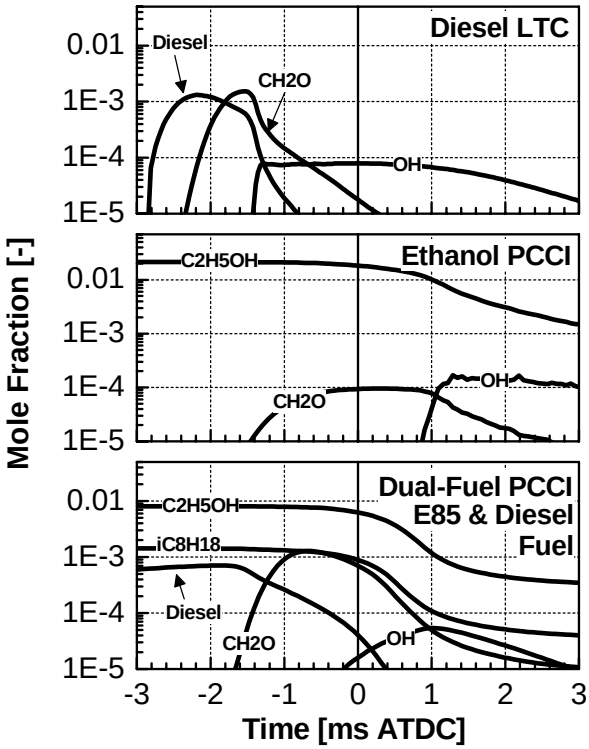

Figure 10. Evolution of several key species for the three combustion strategies. Note that the species evolutions are presented as function of time to account for the differences in engine speed.

Conclusions

CFD modeling results were compared to engine experiments for three different methods of achieving LTC combustion (highly dilute, early injection diesel fuel LTC, early injection ethanol PCCI, and dual-fuel PCCI). It was found that the modeling approach used in this work is capable of capturing the combustion characteristics over this wide range of LTC operation. Furthermore, the changes in combustion characteristics with changing fuel composition were captured well. Comparisons of model predictions with optical engine experiments from the literature [27] showed that the simulations were capable of capturing, not only the

bulk combustion characteristics (e.g., cylinder pressure), but also the details of the injection event (e.g., liquid penetration), as well as the first- and second-stage ignition processes

The ethanol PCCI and dual-fuel PCCI cases showed significantly reduced rates of energy release compared to neat diesel fuel LTC operation. The reduced energy release rates of the ethanol PCCI and dual-fuel PCCI cases may allow these combustion strategies to achieve higher engine loads than diesel LTC.

Based on the modeling results, it appears that the reduced energy release for the ethanol PCCI case is due to thermal stratification generated from the direct injection event. It was found that the combustion event progressed from the leaner-hotter regions to the richer-cooler regions. For the dual-fuel PCCI case, the observed extended combustion duration appears to be the result of a gradient in fuel reactivity generated by the port-fuel-injection of E85 or gasoline and direct-injection of diesel fuel [11]. By comparing the species evolutions, it was found that a very gradual transition to second stage ignition was achieved. This appears to be the result of a staged consumption of the more reactive diesel fuel and less reactive gasoline-ethanol mixture.

Acknowledgements

Financial support from the US Department of Energy (DOE) HCCI contract # DE-FC04-02AL67612 and from the Engine Research Center's Diesel Engine Reduction Consortium (DERC) member companies is gratefully acknowledged.

References

1. G. Bression, D. Soleri, S. Savy, S. Dehoux, D. Azoulay, H. Ben-Hadj Hamouda, L. Doradoux, N. Guerrassi and N. Lawrence, *SAE 2008-01-0034*, 2008.
2. W. L. Hardy and R. D. Reitz, *SAE 2006-01-0026*, 2006.
3. R. Opat, Ra, Y. , Gonzalez D., M.A. , Krieger, R. ,Reitz, R.D., Foster, D.E., Siewert, R. , Durrett, R., *SAE 2007-01-0193*, 2007.
4. M. Sjoberg and J. Dec, *SAE 2008-01-0054*, 2008.
5. V. Manente, P. Tunestal, and B. Johansson, *SAE 2009-01-0944*, 2009.
6. G. T. Kalghatgi, *SAE 2005-01-0239*, 2005.
7. G.T. Kalghatgi, P. Risberg, and H.E. Angstrom, SAE Transactions, 115 (4): 623-634, SAE 2006-01-3385, 2007.
8. P. W. Bessonette, C. H. Schleyer, K. P. Duffy, W. L. Hardy and M. P. Liechty, *SAE 2007-01-0191*, 2007.
9. S. L. Kokjohn, D. Splitter, R. Hanson and R. D. Reitz, *SAE 2009-01-2647*, 2009.
10. R. M. Hanson, S. L. Kokjohn, D. A. Splitter and R. D. Reitz, *SAE 2010-01-0864*, 2010.
11. D.A. Splitter, S.L. Kokjohn, R.M. Hanson, S. Rein, S. Sanders, and R.D. Reitz., *SAE 2010-01-0345*, 2010.
12. A. A. Amsden, "Kiva-3v, Release 2, Improvements to KIVA-3v", LA-UR-99-915, 1999.
13. N. Abani, S.L. Kokjohn, S. W. Park, M. Bergin, A. Munnannur, W. Ning, Y. Sun, and R. D. Reitz, *SAE 2008-01-0970*, 2008.
14. N. Abani, A. Munnannur and R. D. Reitz, *Journal of Engineering for Gas Turbines and Power*, 130(3), 2008.
15. Z. Han and R. D. Reitz, *Combustion Science and Technology*, 106(4-6):267-295, 1995.
16. Y. Ra and R.D. Reitz, "A Combustion Model for IC Engine Combustion Simulations with Multi-Component Fuels", (submitted) *Combustion and Flame*, 2009.
17. Y. Ra, J. E. Yun and R. D. Reitz, *Combustion Science and Technology*, 181:1-29, 2008.
18. S.-C. Kong, Y. Sun and R. D. Reitz, *ASME Journal of Gas Turbines and Power*, 129:245-251, 2007.
19. H. Hiroyasu and T. Kadota, *SAE 760129*, 1976.
20. Y. Sun, *PhD Thesis, University of Wisconsin--Madison*, 2007.
21. M. Frenklach, T. Bowman, G. Smith and B. Gardiner, http://www.me.berkeley.edu/gri-mech/.
22. J. Abraham, *SAE 970051*, 1997.
23. J. C. Beale and R. D. Reitz, *Atomization and Sprays*, 9: 623-650, 1999.
24. A. Munnannur, and R.D. Reitz, *Atomization and Sprays*, 19(7):597–619, 2009
25. P. J. O'Rourke and A. A. Amsden, *SAE 961961*, 1996.
26. P. J. O'Rourke and A. A. Amsden, *SAE 2000-01-0271*, 2000.
27. S. Singh, M. P. B. Musculus and R. D. Reitz, *Combustion and Flame*, 156(10):1898-1908, 2009.
28. M. P. B. Musculus, *SAE Transactions*, 115(3) 83-110, 2006.
29. V. Manente, B. Johansson, P. Tunestal, W. Cannella, *SAE 2010-01-0871*, 2010.
30. D. A. Splitter, R.M. Hanson, S.L. Kokjohn, and R.D. Reitz, *THIESEL 2010 Conference on Thermo- and Fluid Dynamic Processes in Diesel Engines*, Valencia, Spain, September, 2010.
31. T. Lachaux and M. P. B. Musculus, *Proceedings of the Combustion Institute*, 31(2):2921-2929, 2007.
32. K. Hashimoto, *SAE 2008-01-2504*, 2008.
33. K. Hashimoto, *SAE 2007-01-2038*, 2007.
34. S. L. Kokjohn and R. D. Reitz, *11th International Conference on Liquid Atomization and Spray Systems*, Vail, CO, July 2009.
35. J. B. Heywood, "Internal Combustion Engine Fundamentals", McGraw-Hill, New York, 1988.